# Design and experiment of the pneumatic pressure control device for no-till planter

Xinpeng Cao[1,2], Qingjie Wang[1,2*], Hongwen Li[1,2], Jin He[1,2], Caiyun Lu[1,2], Dijuan Xu[3], Xiuhong Wang[1,2]

(1. *College of Engineering, China Agricultural University, Beijing 100083, China*;
2. *Cultivated Land Conservation Agricultural Science Observation and Experiment Station, Northern Hebei Province, Ministry of Agriculture and Rural Affairs, Beijing 100083, China*;
3. *Beijing Vocational College of Agriculture, Beijing 100083, China*)

**Abstract:** An adequate and uniform press wheel pressure is crucial for the homogeneous development of a crop, as it affects actual seeding depth and germination rate. The problems of uneven compaction of seed furrow and consistency of seeding depth can be caused by the pressure fluctuation of the coil-spring pressure control device (CPCD) when the no-till planter is working on the unplowed ground. In this study, a pneumatic pressure control device (PPCD) was designed for the no-till planter, the key structural parameters of air spring for press wheel pressure (PWP) stability were determined by theoretical analysis and parameter calculation. Using the gas-structure coupling finite element simulation method (FESM), the piston radius, piston angle, and cord angle of the air spring are selected as the test factors, and the vertical stiffness was used as the test index to carry out the quadratic rotation orthogonal combination test to establish the regression model of test index and factor. The bench test of the PPCD was carried out under the optimal parameter combination, piston radius of 27.2 mm, piston angle of 11.7°, and cord angle of 30.0°. The vertical stiffness verification test showed that the simulation test was consistent with the bench test result, the vertical stiffness simulation error was 7.1%, and the internal air pressure simulation error was 3.0%; The control response test showed that the average response time of the air spring inflating and deflating was 0.80 s, the maximum overshoot was 4.33% during inflation, and no pressure overshoot during deflation; Under the condition of –40-40 mm surface relief height, the PPCD could effectively reduce the pressure fluctuation compared with the CPCD, and the average reduction of the pressure fluctuation was about 25.1%.

**Keywords:** air spring, no-till planter, pressure control, finite element analysis
**DOI:** 10.25165/j.ijabe.20231603.7670

**Citation:** Cao X P, Wang Q J, Li H W, He J, Lu C Y, Xu D J, et al. Design and experiment of the pneumatic pressure control device for no-till planter. Int J Agric & Biol Eng, 2023; 16(3): 37–46.

## 1 Introduction

No-tillage seeding as the most critical technology of conservation tillage has a series of advantages, such as reducing soil disturbance, inhibiting soil wind and water erosion, and saving agricultural production costs[1-4]. Compared with traditional tillage, no-tillage seeding has no plowing and rotary tillage treatment in the seeding belt. The surface evenness is poor, the soil fluidity is low and the volume is large, which is easy to cause unstable pressure on the press wheel[5-7]. The stable pressure can ensure the proper soil firmness of the seed furrow, make the seeds in close contact with the soil, and play the role of "water transfer" and "moisture preservation", which are directly related to the actual seeding depth, emergence, and yield of crops[8-10]. Therefore, improving press wheel pressure (PWP) stability is an important way to ensure the quality of seeding operation.

To improve the stability of the pressure, the current research is mainly carried out from two aspects: the structure optimization of the press wheel and the precise control of the pressure. In terms of structure optimization, Jia et al.[11] designed an elastic and soil-covered press wheel based on the deformation theory of rubber materials and the research foundation of tire mechanics, improving the stability of the traditional rubber tire press wheel. Guo et al.[12] designed a soil-covering press wheel with two conical structures by analyzing the soil load and movement process of the seed furrow, improving the compaction stability of ridge planting. Wang et al.[13] designed a profiling elastic pressing roller with a built-in symmetrical double-row elastic spoke structure, improving the longitudinal and lateral pressing stability of the press wheel when the surface of the seeding belt is inclined; Zhao et al.[14] designed a press device that realized bidirectional profiling and adjustable press strength, improving the pressure stability during seeding in hilly areas. To solve the problem that soil adhesion on the surface of the press wheel, some scholars optimize the structure of the pressing wheel through bionic and simulation analysis[15,16]. With the improvement of the intelligent level of seeding machines, the active pressure control device plays a significant role in improving the stability of pressure. Li et al.[17] designed a pressure control device with an electric push rod as the working part, which can adjust the

**Received date:** 2022-05-11 **Accepted date:** 2023-02-20
**Biographies: Xinpeng Cao**, PhD candidate, research interest: conservation tillage and equipment, Email: caoxinpeng@cau.edu.cn; **Hongwen Li**, PhD, Professor, research interest: conservation tillage and equipment, Email: lhwen@cau.edu.cn; **Jin He**, PhD, Professor, research interest: conservation tillage and equipment, Email: hejin@cau.edu.cn; **Caiyun Lu**, PhD, Associate Professor, research interest: precision agriculture, Email: lucaiyun@cau.edu.cn; **Dijuan Xu**, MS, Associate Professor, research interest: facility agriculture, Email: 82109@bvca.edu.cn; **Xiuhong Wang**, PhD candidate, research interest: conservation tillage and equipment, Email: wangxiuhong@cau.edu.cn.
***Corresponding author: Qingjie Wang**, PhD, Professor, research interest: conservation tillage and equipment. College of Engineering, China Agriculture University, No.17, Qinghua East Road, Haidian District, Beijing 100083, China. Tel: +86-10-62737300, Email: wangqingjie@cau.edu.cn.

pressure according to the crops and requirements; Bai et al.[18] realized the control of PWP by adjusting the elongation of the profiling coil-spring at the press device by the hydraulic cylinder and designed a hydraulic pressure control device. In the existing research, hydraulic cylinders or push rods are used as actuators to directly or indirectly push the press wheel to realize the adjustment of the PWP. However, in the no-tillage surface with poor surface evenness, the pressure fluctuation cannot be effectively suppressed and the pressure stability cannot be improved.

In view of the above problems, this paper selects air spring as the working part, improving the stability of the pressure under the same ground fluctuation conditions without changing the structure of the press wheel. At the same time, the pressure can be adjusted by changing the internal pressure of the air spring to achieve accurate control of the pressure. The optimal combination of structural parameters of the air spring is determined through theoretical analysis and finite element simulation, to improve the stability of the PWP. The operation performance of the pneumatic pressure control device (PPCD) is further verified through field tests.

## 2 General structure and working principle

### 2.1 General structure

PPCD was mainly designed for the pressure regulation of seeding belts under no-tillage seeding operation. Its structure is shown in Figure 1, mainly composed of connecting frame, angle sensor, air spring, press wheel mounting frame, and press wheel.

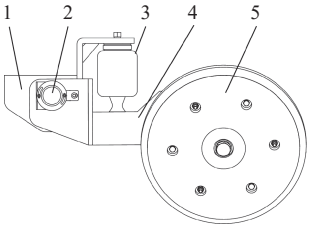


1. Connecting frame 2. Angle sensor 3. Air spring 4. Press wheel mounting frame 5. Press wheel

Figure 1 Structure diagram of the PPCD

### 2.2 Working principle

As shown in Figure 2, the PPCD was rigidly connected with the seeding unit through the connection frame, the head of the air spring was fixed with the connecting frame, and the foot was fixed with the press wheel mounting frame. The pressure was adjusted by pushing the press wheel mounting frame through the foot of the air spring. The outer shell of the angle sensor was fixed with the press wheel mounting frame, and the internal axis was fixed with the connecting frame, the angle change of the press wheel mounting frame relative to the seeding unit was measured, and then the height of the air spring was detected. The air pressure sensor was installed in the inflating and deflating pipes of the air spring to detect the air pressure inside the air spring. The electric proportional valve was installed between the air supply device and the air spring. By inflating and deflating the air spring, the internal air pressure of the air spring was adjusted to realize the adjustment of the output force of the air spring, thereby realizing the adjustment of the pressure.

Before seeding, the PWP was set by the pressure control unit according to the ground conditions and agronomic requirements of the seeding area. The pressure control unit regulated the initial pressure by controlling the electric proportional valve to inflate and deflate the air spring. During the seeding, the control unit read the internal air pressure of the air spring through the air pressure sensor, calculated the height of the air spring through the angle sensor, and then calculated the PWP. When the average pressure was greater than the set value, the air spring was deflated through the electric proportional valve to reduce the output force of the air spring, and conversely, the air spring was inflated, so as to realize the control of the PWP. The PPCD can adapt to different crops by changing the press wheel and adjusting the pressure.

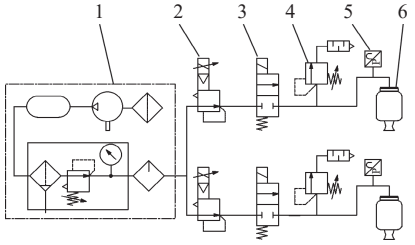


1. Air supply device 2. Electric proportional valve 3. Solenoid valve 4. Pneumatic relief valve 5. Air pressure sensor 6. Air spring

Figure 2 Pneumatic circuit diagram of PPCD

## 3 Design and analysis of key components

The air spring was the main working part of the PPCD. During the seeding operation, the pressure control unit inflated and deflated the air spring through the electric proportional valve to adjust the PWP, and calculated the pressure by detecting the internal air pressure and height of the air spring.

### 3.1 Force analysis of press control device

In order to determine the relationship between the output force of the air spring and the PWP, the force of the press control device was analyzed in this study. The front section of the PPCD was fixed with the seeding unit, and the rear press wheel contacted the surface of the seeding belt to cover and press the seed furrow. During the seeding, the press wheel followed the ups and downs of the seed belt surface, and the pressure on the ground was mainly determined by the action of the air spring on the press wheel mounting frame.

The force analysis of PPCD is shown in Figure 3, the horizontal output force of the air spring was offset by the reaction of the

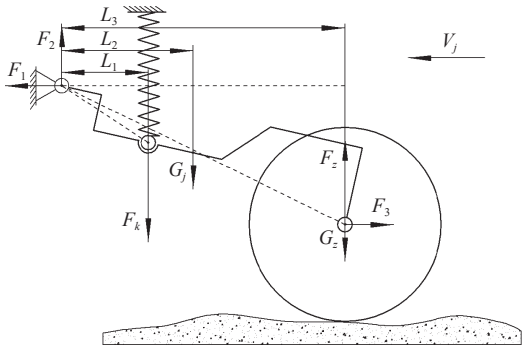


Note: $F_1$ is the tractive force of the seeding monomer to pressure device, N; $F_2$ is the vertical support force of the seeding monomer to pressure device, N; $F_3$ is the tractive resistance of the ground to pressure device, N; $F_k$ is the vertical force of the air spring to press wheel mounting frame, N; $G_j$ is the gravity of the press wheel mounting frame, N; $Gz$ is the gravity of the press wheel, N; $L_1$ is the horizontal distance between the mounting point of air spring and the installation shaft of pressure device, m; $L_2$ is the horizontal distance between the centroid of the crushing wheel mounting frame and the installation shaft of pressure device, m; $L_3$ is the horizontal distance between the mounting shaft of the press wheel and press device, m; $V_j$ is the forward velocity of the machine, m/s.

Figure 3 Force analysis of PPCD

seeding unit. The output force along the vertical direction was the main factor affecting the pressure, so the vertical force of the press device was mainly analyzed.

Taking the axis of the press device mounting shaft as the rotation center, the moment balance equation can be obtained.

$$F_z = \frac{F_k L_1 + G_j L_2 + G_z L_3}{L_3} \tag{1}$$

From Equation (1), when the size and installation form of the press wheel and the press wheel mounting frame were determined, the amount of change in the PWP can be determined by the output force of the air spring.

Taking the position of the pressing wheel while mounting frame was horizontal as the initial working position, when the surface relief height was $\Delta x$, the pressure change amount can be obtained by Equation (1).

$$\Delta F_z = \frac{k \Delta x L_1}{L_3} \tag{2}$$

where, $\Delta F_z$ is the pressure variation, N; $k$ is the vertical stiffness of air spring, N/m; $\Delta x$ is the surface relief height, m.

From the above analysis, when the surface relief height was the same, the PWP change amount was inversely proportional to the distance $L_3$, and was directly proportional to the horizontal distance $L_1$. When the position of the press wheel was fixed, the fluctuation of the pressure was determined by the vertical stiffness of the air spring. Therefore, a nonlinear mechanical model of the air spring was established to analyze the vertical stiffness of the air spring.

### 3.2 Nonlinear mechanical model of air spring

The air spring deformed during the press operation and its elastic deformation was realized by the rubber skin curling along the outer surface of the piston to compress the internal air. During the deforming process, the internal air pressure and volume changed at the same time, which had obvious nonlinear characteristics. According to the structure, air springs can be divided into two types: rolling lobe and bellow type air spring. Compared with bellow type air springs, rolling lobe air springs had the characteristics of easy adjustment of load-bearing characteristics and low natural frequency. Therefore, a rolling lobe air spring was selected as the working part. The structure of the rolling lobe air spring is shown in Figure 4, which was mainly composed of upper cover plate, press ring, rubber skin, and piston.

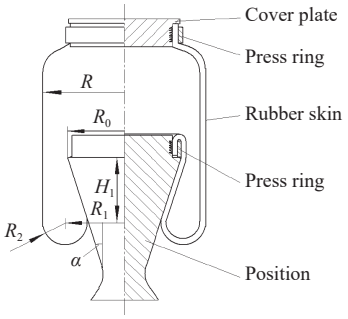


Note: $R$ is the inner radius of rubber skin, m; $R_0$ is the radius of piston head; $R_1$ is the radius of roll ear center, m; $R_2$ is the radius of roll ear, m; $H$ is the effective piston height, m; $\alpha$ is the angle of the piston, (°).

Figure 4 Structure diagram of rolling lobe air spring

The existing research results showed that the bearing capacity of the air spring was mainly affected by the internal air pressure and the effective area, the specific relationship was

$$F_k = pA_e \tag{3}$$

where, $F_k$ is the vertical load of air spring, N; $p$ is the internal air pressure of air spring, MPa; $A_e$ is the effective area of air spring, m$^2$.

$$A_e = \pi(R - R_2)^2 \tag{4}$$

When the height of the press wheel changed, the air spring was compressed or stretched internally, and the internal volume and pressure of the rubber skin satisfy the gas state equation

$$(p + p_a) V^{\lambda} = (p_0 + p_a) V_0^{\lambda} \tag{5}$$

where, $p_0$ is the internal pressure of the air spring at a certain time, MPa; $V$, $V_0$ is the internal volume of the air spring at the initial state and a certain time, m$^3$; $\Delta x$ is the surface relief height, m; $\lambda$ is a variable index, when the air spring runs at a low frequency lower than 0.1 Hz, $\lambda$=1, and when the high frequency is higher than 30 Hz, $\lambda$=1.4. In practice, according to the working conditions of the repressing wheel, $\lambda$=1.33[19].

Substituted Equation (5) into Equation (3), the output force in the vertical direction of the air spring was obtained as

$$F_k = \left[ \left( \frac{V_0}{V} \right)^{\lambda} (p_0 + p_a) - p_a \right] A_e \tag{6}$$

The vertical dynamic stiffness expression of the air spring can be obtained by deriving the vertical deformation of Equation (5).

$$k = \frac{\lambda A_e (p_0 + p_a)}{V} \frac{dV}{dx} + p_0 \frac{dA_e}{dx} \tag{7}$$

It can be seen from the above Equation that the stiffness change of the air spring can be divided into the change caused by the internal volume and the effective area. The vertical stiffness of the air spring was mainly related to the volume and volume change rate, the effective area and the area change rate, and the internal air pressure. The rolling lobe air springs mainly adjusted the air spring volume and effective area by adjusting the parameters of the rubber skin and the piston, thereby realizing the adjustment of the air spring stiffness.

### 3.3 Structural parameter of air spring

#### 3.3.1 Design of piston

The shape of the air spring piston is shown in Figure 5. There were mainly four main structural forms, such as cylinder, cone, turbination, and curve. In the process of elastic deformation of the air spring, the rubber skin appressed the piston surface under the action of the internal air pressure. With the change of the contact point between the rubber skin and the piston surface, the effective area and the change rate of the effective area changed. Adjusting the stiffness characteristics of the air spring by changing the piston size

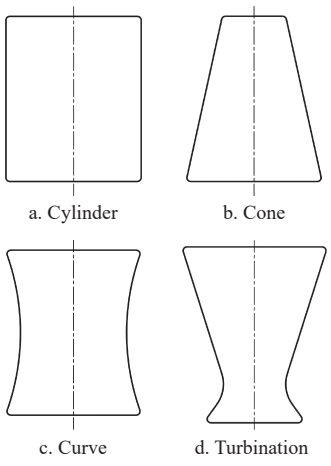


Figure 5 Piston shape of rolling lobe air spring

under different structural forms of the rolling lobe air spring was the main stiffness adjustment method at present.

It can be seen from Figure 5 that when the shape of the air spring piston was cylindrical, the piston angle $\alpha$=0, the change of effective area was 0, and the stiffness of the air spring was only determined by the internal air pressure; When the air spring was conical, the piston angle $\alpha$>0, the effective area of the air spring increased with the compression of the air spring, and the stiffness increased; When the piston was curved, the piston angle changed with the change of height, the air spring stiffness first decreases and then increases; When the piston shape was turbination, the piston angle $\alpha$<0. With the compression of the air spring, the effective area of the air spring decreased, and the effective area change rate was negative. The turbination shape was conducive to reducing the stiffness of the air spring and reducing the fluctuation of the PWP. Therefore, the shape of the air spring piston was selected as turbination. The parameters of the turbination shape piston were analyzed, and the structural parameters of the piston are shown in Figure 6.

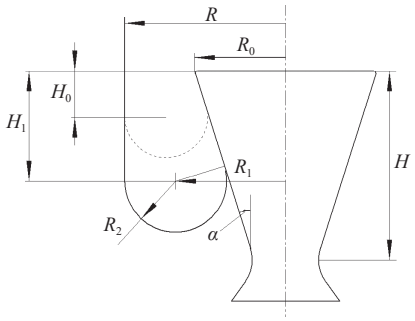


Note: $H$ is the total effective piston height, m; $H_0$ is the effective piston height at the initial position, m.

Figure 6 Structure parameter of conic shape piston

When the air spring roll ear moved from the height $H_0$ to $H_1$, it can be seen from Equation (4) that the effective area of the air spring gradually increased, which is determined by the geometric relationship, the geometric relationship

$$R_r = R_0 - H_1\tan\alpha + R_2\sec\alpha \tag{8}$$

where, $R_r$ is the effective bearing radius of the air spring, m.

where,

$$R = R_r + R_2 \tag{9}$$

Substituted Equation (9) into Equation (8), then

$$R_r = R_0 + \frac{R - R_0}{1 + \cos\alpha} - H_1 \tan\left(\frac{\alpha}{2}\right) \tag{10}$$

From Equation (10) got that when the inner radius of rubber skin $R$ remained unchanged, the effective bearing radius $R_r$ was positively correlated with the diameter $R_0$ of the piston head, and negatively correlated with the effective piston height $H_1$ and the piston angle $\alpha$.

Combined with the existing research and field test measurements, the adjustment range of the PWP during the no-tillage seeding was determined as 200-500 N, and the adjustment range of the height of the repression wheel was 150 mm[20].

Under the condition that the position of the pressing wheel was kept unchanged, to reduce the fluctuation of the PWP, known from Equation (2) that the horizontal distance $L_1$ shall be minimized. Combined with the installation position of the air spring, the $L_1$ of the final working position was determined to be 110 mm, which was 40% of the distance $L_3$. From this, the maximum vertical output force of the air spring was calculated to be 1000 N, the minimum force was 250 N, the total action height $H$ of the air spring piston was 60 mm, and the maximum torsion angle of the piston was 15.3°.

According to Equations (3) and (4), the output force of the air spring was determined by diameter $R$ and pressure $p$. In order to prevent the rubber skin from being involved between the piston and the cover plate, the minimum air pressure inside the bladder shall be higher than 0.05 MPa[21]. During the deformation process of the air spring, it was necessary to ensure that the piston not contacted the inner surface of the rubber skin. Combined with the maximum torsion angle of the piston of 15.3° and the total action height of 60 mm, the minimum distance between the piston head and the inner surface of the rubber skin was calculated to be 16.4 mm. Since there was no derivable relationship between the diameter of the piston, the bearing capacity, and pressure[22], to ensure that the minimum output force meets the requirements of the PWP adjustment range, estimated according to Equations (3), (4) and (9) that the maximum inner diameter of the inflated rubber skin was 48 mm. Combined with the expansion ratio of the air spring after inflation of 1.2-1.8[22], the calculated range of the radius $R_0$ was 27-40 mm. According to the radio of piston head $R_0$, the total effective piston height $H$ and the minimum radius 5 mm of the piston base, the range of piston angle $\alpha$ was 0°-20°.

3.3.2 Design of rubber skin

The rubber skin of the air spring was composed of rubber and cord layers, which the cord layer is the core component of the rubber skin. The cord takes over most of the force of the air spring and plays a key supporting role in the rubber skin structure. The structure of the rubber skin is shown in Figure 7, the structural parameters that affected the bearing characteristics of the air spring mainly included the cord spacing, the distance between the cord layers, the number of cord layers, the angle and radius of the cord and the thickness of the rubber.

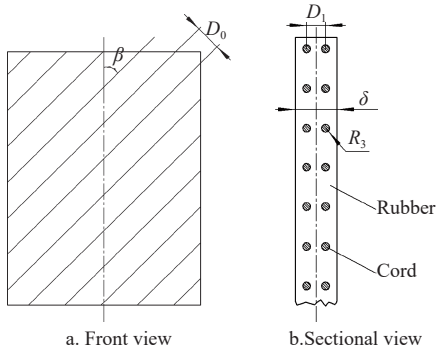


Note: $D_0$ is the cord spacing, m; $D_1$ is the distance between cord layer, m; $\delta$ is the thickness of rubber skin, m; $R_3$ is the radius of cord, m; $\beta$ is the angle of cord, (°).

Figure 7 Structure parameter of rubber skin

The cord angle was the angle between the cord and the meridian of the air spring, and the angle between adjacent cord layers was 90°. Compared with the structural parameters such as the spacing and quantity of the cord layers, the cord angle had the most significant effect on the vertical stiffness of the air spring[23]. To ensure the lateral and vertical stability of the air springs, the angle of the cord was usually 30°-60°[24]. Based on the existing air spring piston radio and internal working air pressure, combined with the existing processing technology and experience, the $\delta$ was selected as 2.5 mm, the $D_1$ was 1 mm, and the number of cord layers was 2,

the $R_3$ was 0.25 mm, and the $D_0$ was 1 mm.

## 4 Simulation analysis and parameter optimization

The ABAQUS finite element simulation has been widely used to simulate and analyze the mechanical characteristics of air springs in high-speed trains, buses, and heavy trucks, and its modeling effectiveness and accuracy have been verified many times[25,26]. Meanwhile, before the research of this article, the vertical force, pitch diameter, and internal pressure of the simulation model and the physical model have been verified in detail in the previous research[27]. To obtain data under actual working conditions and determine the optimal parameter combination, the nonlinear finite element software ABAQUS was used to analyze the output force of the air spring during the seeding.

### 4.1 Finite element model

#### 4.1.1 Material of model

When establishing the FESM of the air spring in ABAQUS (Figure 8), the air spring can be simplified into four parts: the rubber skin, the gas in the cavity, the upper cover plate, and the bottom piston, according to the force and deformation. The rubber skin was made of rubber and cord. The Mooney-Rivlin model was used to simulate the nonlinear elasticity of the rubber material. The material parameter $C_{10}$ was 0.5178 MPa and $C_{01}$ was 0.1426 MPa[24]. The rebar unit was used to simulate the cord layer in the rubber skin, and the cord was embedded in the rubber material. The spacing of the cords was simulated by the spacing of the rebar; the distance of the cord layers was simulated by the distance between the neutral plane and the rebar; the cord radius was defined by the cross-sectional area of the rebar. The cord angle was simulated by the rebar unit angle, Young's modulus of the cord material was 7200 MPa, and Poisson's ratio was 0.31[24]. The cavity model was used to simulate the gas in the cavity. The cover plate and the piston of the air spring were regarded as rigid bodies.

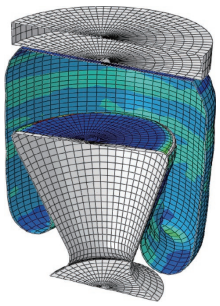

Figure 8 Finite element model of air spring

#### 4.1.2 Contact and boundary of model

The BEAM function was used to connect the reference point of the piston with the installation shaft of the PPCD. The deformation of the air spring during the seeding were simulated by the rotation of the piston around the center point of the mounting shaft. Based on the TIE tool, the repeated nodes of the rubber skin fluid element were fixed to reference points of the cover plate and the piston. The contact between the deformed rubber skin and the cover plate and the piston was defined as non-slip contact. The rubber skin, the upper and lower surfaces formed a closed cavity, and the air was inflated in the cavity.

#### 4.1.3 Meshing and step definition

The rubber skin was simplified as a shell element, and the rubber skin shell element was simulated by the S4R element. The thickness of the shell was the same as the rubber skin, the cord layer was embedded in the shell, and the mesh was generated by sweeping, the mesh size was 3 mm. The cover plate and piston were shelled as discrete rigid, and the S4R mesh unit was generated by sweeping, the mesh size was 3 mm.

The air spring loading process can be divided into two steps. The first step is the inflation process, constraining the degree of freedom of the piston. While inflating the fluid chamber in the rubber skin, the cover plate compresses the rubber skin to the middle working position of the air spring, the internal air pressure is 0.3 MPa in the meantime. The second step is to constrain the degree of freedom of the cover plate, and disconnect the air source of the fluid chamber, the internal pressure changes with the volume of the fluid chamber. Driving the piston to rotate around the installation shaft of the pressure device to deflect the piston to 10 mm in the vertical direction, then the internal pressure of the fluid chamber, the displacement of the piston, and the vertical force of the cover plate were recorded during the deflection process.

### 4.2 Optimizing index

The design objective of the PPCD was to improve the stability of the PWP under the conditions of no-till sowing. The vertical stiffness of the air spring under different structural parameters determined the stability of the PWP, and its vertical stiffness was calculated according to Equation (11).

$$k_{sy} = \frac{F_{y1} - F_{y0}}{\Delta y} \tag{11}$$

where, $k_{sy}$ is the vertical stiffness of the air spring in simulation, N/m; $F_{y1}$, $F_{y0}$ is the output force of the air spring in different positions, N; $\Delta h$ is the vertical height change of the air spring, m.

### 4.3 Analysis of simulation result

#### 4.3.1 Design of orthogonal experimental

Carried out (three factors) quadratic orthogonal rotation combination test, selected the piston radius, piston angle, and cord angle determined by theoretical analysis as test factors. In order to verify the results of the theoretical analysis, the significance level of the factor on the index was determined, and the range of each parameter according to the actual needs was optimized.

The test factors and levels are listed in Table 1, and the test scheme and result analysis are listed in Table 2.

**Table 1 Experimental factors and levels**

| Level | Piston radius $X_1$/mm | Piston angle $X_2$/(°) | Cord angle $X_3$/(°) |
|---|---|---|---|
| +γ | 40.0 | 26.0 | 60.0 |
| +1 | 37.6 | 20.7 | 53.9 |
| 0 | 34.0 | 13.0 | 45.0 |
| −1 | 30.4 | 5.3 | 36.1 |
| −γ | 27.0 | 0.0 | 30.0 |

Note: Number of tests for the center point is 9 times.

#### 4.3.2 Regression analysis and significance test

The Design Expert 10.0.7 software was used for quadratic regression analysis of the results, and multiple regression fitting was carried out. The regression equation of stiffness $Y$ was obtained as shown in Equation (12), and its significance was tested.

The vertical stiffness of the air spring after excluding insignificant factors is shown in Table 3, and the test model was extremely significant ($p$<0.01). Among the main factors, the air spring piston radius, piston angle, and cord angle had extremely significant effects on the vertical stiffness ($p$<0.01). In the interaction term, piston radius and cord angle had significant effects on vertical stiffness (0.01<$p$<0.05), and piston radius and piston angle had significant effects on vertical stiffness (0.05<$p$<0.1). In

**Table 2 Test plan and experimental result**

| Test No | Piston radius $X_1$/mm | Piston angle$X_2$/(°) | Cord angle$X_3$/(°) | Vertical stiffness $Y$/N·mm$^{-1}$ |
|---|---|---|---|---|
| 1 | 29.6 | 4.1 | 36.1 | 15.2 |
| 2 | 37.4 | 4.1 | 36.1 | 29.4 |
| 3 | 29.6 | 15.9 | 36.1 | 12.8 |
| 4 | 37.4 | 15.9 | 36.1 | 22.6 |
| 5 | 29.6 | 4.1 | 53.9 | 13.9 |
| 6 | 37.4 | 4.1 | 53.9 | 20.6 |
| 7 | 29.6 | 15.9 | 53.9 | 8.5 |
| 8 | 37.4 | 15.9 | 53.9 | 7.7 |
| 9 | 27.0 | 10.0 | 45.0 | 7.9 |
| 10 | 40.0 | 10.0 | 45.0 | 25.5 |
| 11 | 33.5 | 0.0 | 45.0 | 23.3 |
| 12 | 33.5 | 20.0 | 45.0 | 17.1 |
| 13 | 33.5 | 10.0 | 30.0 | 18.4 |
| 14 | 33.5 | 10.0 | 60.0 | 11.4 |
| 15 | 33.5 | 10.0 | 45.0 | 14.4 |
| 16 | 33.5 | 10.0 | 45.0 | 10.4 |
| 17 | 33.5 | 10.0 | 45.0 | 13.9 |
| 18 | 33.5 | 10.0 | 45.0 | 10.6 |
| 19 | 33.5 | 10.0 | 45.0 | 12.6 |
| 20 | 33.5 | 10.0 | 45.0 | 10.4 |
| 21 | 33.5 | 10.0 | 45.0 | 10.4 |
| 22 | 33.5 | 10.0 | 45.0 | 10.5 |
| 23 | 33.5 | 10.0 | 45.0 | 13.6 |

the quadratic term, the piston angle had an extremely significant effect on the vertical stiffness ($p$<0.01), and the piston radius had a significant effect on the vertical stiffness (0.01<$p$<0.05). The Primary and secondary sequence of factors on the vertical stiffness was $X_1$, $X_3$, and $X_2$. After incorporating the insignificant factors into the residue term, the variance analysis was performed again, and the regression equation between each factor and the index was obtained.

**Table 3 Variance analysis for vertical stiffness**

| Source | Sum of squares | Freedom | Mean square | $F$-value | $p$-value |
|---|---|---|---|---|---|
| Model | 691.93 | 7 | 98.85 | 19.8 | <0.0001 |
| $X_1$ | 257.48 | 1 | 257.48 | 51.58 | <0.0001 |
| $X_2$ | 105.13 | 1 | 105.13 | 21.06 | 0.0004 |
| $X_3$ | 123.78 | 1 | 123.78 | 24.8 | 0.0002 |
| $X_1X_2$ | 17.58 | 1 | 17.58 | 3.52 | 0.0801 |
| $X_1X_3$ | 41.41 | 1 | 41.41 | 8.29 | 0.0114 |
| $X_1^2$ | 33.4 | 1 | 33.4 | 6.69 | 0.0206 |
| $X_2^2$ | 113.99 | 1 | 113.99 | 22.84 | 0.0002 |
| Residual | 74.88 | 15 | 4.99 | | |
| Lack of fit | 51.25 | 7 | 7.32 | 2.48 | 0.1133 |
| Total value | 766.81 | 22 | | | |

$$Y = -10.010\,04 - 1.764\,36X_1 + 0.179\,34X_2 + 1.873\,34X_3 - 0.064\,510X_1X_2 - 0.065\,997X_1X_3 + 0.097\,056X_1^2 + 0.075\,756X_2^2 \quad (12)$$

The above regression equation was tested for lack of fit, as listed in Table 3. The results of lack of fit indicated that the verification results were not significant ($p$>0.1), which proved that there was a significant quadratic relationship between the test index and factor.

4.3.3 Response surface analysis

Through data processing, the response surface of the interaction between significant factors to the vertical stiffness was obtained, as shown in Figure 9.

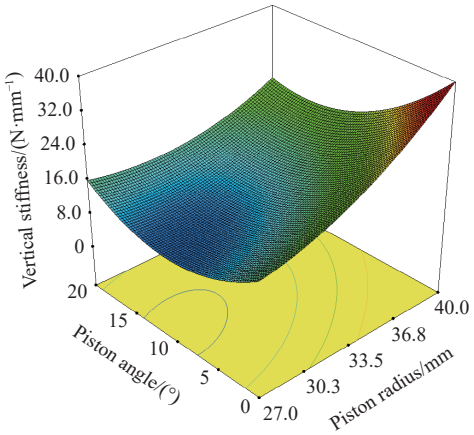


a. Effects of piston radius and piston angle on vertical stiffness

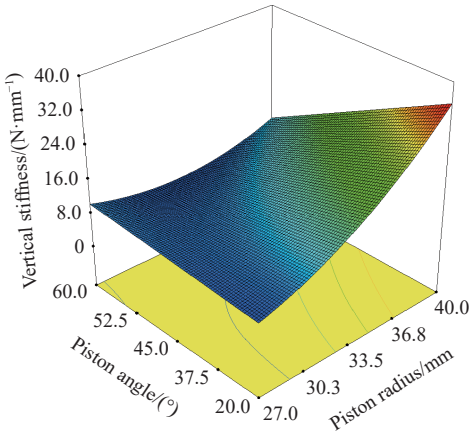


b. Effects of piston radius and cord angle on vertical stiffness

Figure 9 Effects of interaction factors on vertical stiffness

It can be seen from Figure 9a that for the piston radius, when the piston angle was small, the vertical stiffness of the air spring increased significantly with the increase of the piston radius, the effect reduced gradually but still showed a positive gain. For the piston angle, the vertical stiffness first decreased and then increased with the increase of the piston angle under different piston radii. It can be seen from Figure 9b that for the cord angle, when the piston radius was small, the vertical stiffness of the air spring decreases with the increase of the cord angle. With the continuous increase of the piston radius, the influence of the cord angle on the vertical stiffness changes from a negative to a positive effect, and the increase of the cord angle can significantly reduce the vertical stiffness of the air spring.

### 4.4 Parameter optimization of air spring

In order to obtain the best structural parameters of the air spring, the optimization module of Design Expert 10.0.7 was used to optimize the constraint objective of the regression model. The optimization constraint conditions, objectives, and constraint functions were selected according to the actual operation and related theories.

$$\begin{cases} \min Y(X_1, X_2, X_3) \\ \text{s.t.} \begin{cases} 27\ \text{mm} \le X_1 \le 40\ \text{mm} \\ 0^\circ \le X_2 \le 20^\circ \\ 30^\circ \le X_3 \le 60^\circ \end{cases} \end{cases} \quad (13)$$

The objective function was optimized and calculated according

to the principle of reducing vertical stiffness, ensuring service life, and reducing the volume of the air spring. According to the influence rule of piston radius, piston angle, and cord angle on vertical stiffness obtained by the orthogonal simulation test in section 4.3.3. Combined with the installation space of the press device, the optimization results obtained with a combination of the piston radius of the air spring of 27.2 mm, piston angle of the truncated cone of 11.7°, cord angle of 30.0°, and the vertical stiffness of 8.1 N/m. The test was carried out again according to the optimized results, and the vertical stiffness of the air spring during the torsion process was 8.5 N/mm, which was consistent with the optimized results.

## 5 Materials and methods

### 5.1 Developed test platform for press wheel

Based on simulation results and parameter optimization design, an air spring with a piston radius of 27.2 mm, piston angle of 11.7°, and cord angle of the rubber skin of 30.0° was processed. The test was carried out on the performance test bench of the press wheel in the Conservation Tillage Research Center of the Ministry of Agriculture and Rural Affairs. The test bench was used to simulate the surface relief height of the press wheel during the no-tillage seeding, and the pressure fluctuation of the press wheel was recorded. The test bench is shown in Figure 10, the test bench was compatible with the coil-spring pressure control device (CPCD). During the test, the PWP was recorded by the cantilever beam pressure sensor (Dayang, Bengbu, China) in the pressure measurement unit; Adjusted the internal pressure of the air spring through an electric proportional valve (SMC, Kyoto, Japan); Recorded the changes of air pressure inside the air spring by an air pressure sensor (Siemens, Munich, Germany); The height change of the repression wheel was recorded by a displacement sensor (Milai, Taizhou, China). All data were collected and recorded by NI-6002 data acquisition card (National Instruments, Austin, USA).

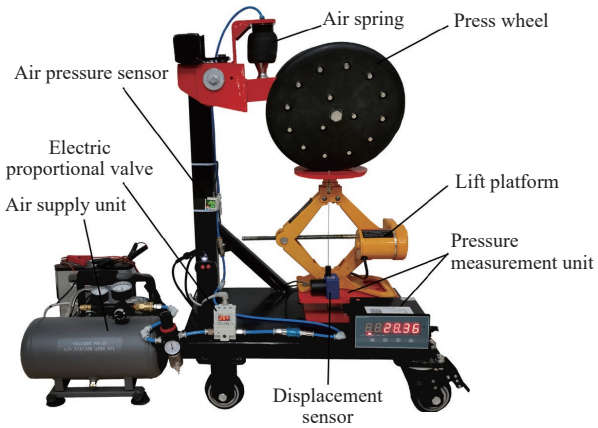


Figure 10 Performance test bench of press wheel

### 5.2 Experiments

5.2.1 Vertical stiffness verification

During the test, adjusted the position of the pressing wheel to the middle position, which was the horizontal position of the pressing wheel mounting frame. Adjusted the internal air pressure of the air spring through the electric proportional valve, which was the same pressure of 0.3 MPa in the simulation test. Used the lifting platform to adjust the press wheel to rise by 25 mm, at this time, the vertical displacement of the air spring piston was the same as the simulation test, which was 10 mm. During the test, the data was recorded every time the pressing wheel was raised by 5 mm, and the PWP during the lifting process was recorded through the pressure measurement unit and the vertical output force of the air spring can be calculated. Also, the air pressure inside the air spring was recorded through the air pressure sensor. The vertical characteristic output curve of the air spring of the press wheel was obtained and compared with the simulation test.

5.2.2 Control response test

During the seeding, the air spring of the press wheel needed to adjust the internal air pressure of the air spring according to the operation requirements to realize the adjustment of the PWP, its response characteristics represent the control performance of the device. In the test, the working height of the air spring was 125 mm and the air pressure was 0.3 MPa as the starting point for pressure adjustment, and the air spring was charged and discharged through an electric proportional valve to perform a pressure control step response test. To ensure the continuity and accuracy of data acquisition, set the sampling frequency of the data acquisition card for the internal pressure of the airbag as 100 Hz and the sampling time as 5 s. After sampling, screened the valid data for 2 s in combination with the sampling results.

5.2.3 Comparison of the PWP fluctuation

To compare the PWP of the PPCD and the CPCD under the condition of different surface relief heights, the two devices were installed on the test bench for the performance of the press wheel. During the test, ensure that the press wheel mounting frame at the starting position was level, and the PWP was the same when the spring did not act by adjusting weight. According to the average surface relief height of the no-tillage seeding measured in the field, the height fluctuation of the press was adjusted using the lifting platform to be –40 mm, –20 mm, 0 mm, 20 mm, and 40 mm, respectively. First, the test of CPCD was carried out as shown in Figure 11, and the PWP adjustment handle was pushed into the slot gears 1 to 4, respectively, and the PWP in 4 different hand positions was measured under different surface reliefs. After replacing the PPCD, adjusting the PWP in the initial position is the same as the pressure in 4 different gears respectively through the electric proportional valve. After the adjustment was completed, disconnect the air spring from the external air source, and the internal pressure of the air spring fluctuated with the height of the press wheel. Recorded the PWP of the PPCD at different heights, and compare it with the CPCD.


Figure 11 Performance test of the CPCD

## 6 Results and discussion

### 6.1 Vertical stiffness and pressure error

The vertical stiffness verification test results are shown in Figure 12. When the internal air pressure of the air spring at the initial position was 0.3 MPa, the vertical output force of the air spring has the same trend as the internal air pressure and the maximum error range was within 10%. Among them, the average vertical stiffness during the compression process was 9.3 N/mm, and the error with the simulation test was 7.1%; The maximum

internal air pressure difference was 0.01 MPa, and the error with the simulation test was 3.0%. The verification test results showed that the vertical stiffness change during the torsional deformation of the air spring can be simulated by the finite element gas-solid coupling simulation method, and the error between the simulation results and the bench test results was within the acceptable range.

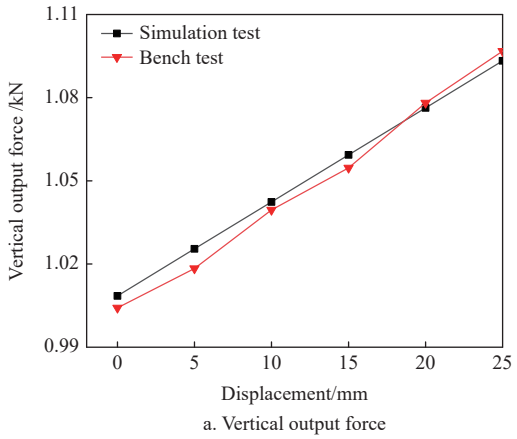


a. Vertical output force

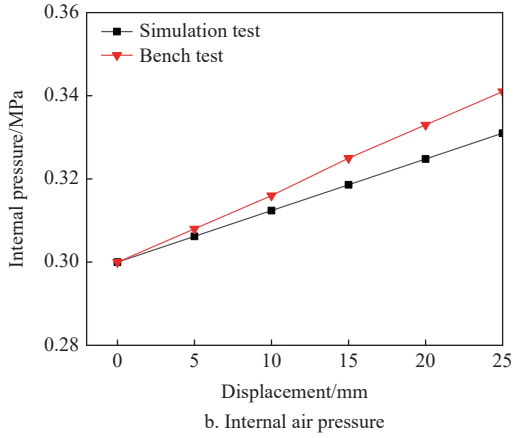


b. Internal air pressure

Figure 12 Comparison of air spring bench and simulation test

### 6.2 Effect of pressure difference on response time

The test results of the air spring inflating and deflating response are shown in Figure 13, when the internal pressure of the air spring was adjusted by the electric proportional valve, the pressure regulation was fast and there was no large pressure oscillation. When the air spring was inflated, the internal pressure overshot, the maximum overshoot did not increase significantly with the increase of the target pressure, and the maximum overshoot was 4.33%. The inflation response time increased with the increase of the target and initial pressure difference, and the response time increased by 0.13 s on average for every 0.1 MPa increase in the pressure difference. When the air spring was deflated, there was no overshoot of the pressure. The deflation response time was less than the inflation response time, and the average response time was 0.56 s when the pressure difference was 0.2 MPa. When the initial air pressure was 0.3 MPa, the average response time of the air spring inflating and deflating was 0.80 s.

When the air spring was inflated and deflated under the same pressure difference through the electric proportional valve, the inflation response time to achieve stable pressure was significantly longer than the deflation time. Therefore, in order to improve the speed of pressure adjustment at the beginning of the seeding, the air spring should be over-inflated, and the pressure could be quickly adjusted by deflation. At the same time, the optimal inflation time under different pressure differences could be determined by establishing the inflation response time model. By limiting the working time of the electric proportional valve, the overshoot of the internal pressure of the air spring could be prevented. In this way, the inflating response speed can be improved at the same time.

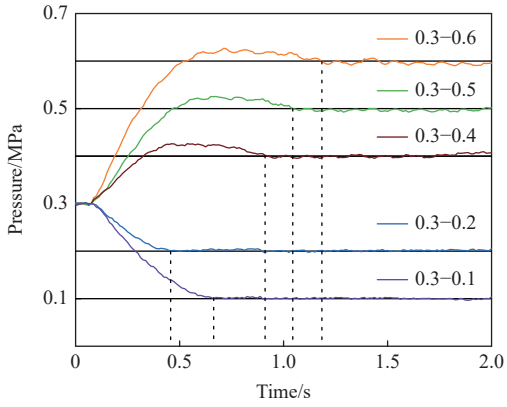


Figure 13 Air spring inflating and deflating response test

### 6.3 Effect of surface relief height on the PWP

The PWP fluctuation of the PPCD and the CPCD under different initial pressure under different surface relief heights is shown in Figure 14. The test results showed that different surface relief heights, adjustment gears, and types of press devices affected the PWP and its stability. The PWP of the PPCD and CPCD increased with the surface relief height and decreased as the height decreased. Surface relief had a very significant effect on the press force stability of the CPCD ($p$<0.01), and had a significant effect on the press force stability of the PPCD (0.05<$p$<0.1). Compared with the coil spring, the air spring can reduce the significant level of the PWP fluctuation caused by the surface relief height and improve the stability of the PWP.

The PWP stabilization effect of the PPCD was better when the ground height was lowered than raised. The reason was that as the height of the ground increased, the height of the air spring decreased, the air inside the spring was compressed, and the internal pressure increased, which increased its vertical stiffness. When the ground relief height was ±40 mm, the average vertical stiffness of the press device in different gears is listed in Table 4. The PPCD using the air spring reduced the stiffness of PWP by 17.8%, 19.3%, 26.1%, and 37.3% in gear positions 1 to 4 compared with the CPCD, respectively. The PWP fluctuation was reduced by 25.1% on average. With the increase of the set press force, the stability improvement effect of the PPCD was more obvious.

Using air spring instead of coil spring can significantly reduce the fluctuation of the PWP during the seeding, and achieved better pressure stability. Future studies should be focused on developing different control methods, such as real-time adaptive PID and fuzzy hybrid controller in association with the air spring models, to improve the pressure stability in different ground relief heights and soil conditions.

## 7 Conclusions

A pneumatic pressure control device using air springs for pressure control was developed for the no-till planter. The press wheel pressure (PWP) was adjusted by inflating and deflating to the air spring, thereby improving the stability of the PWP during the no-tillage seeding.

Taking the vertical stiffness of the air spring during the

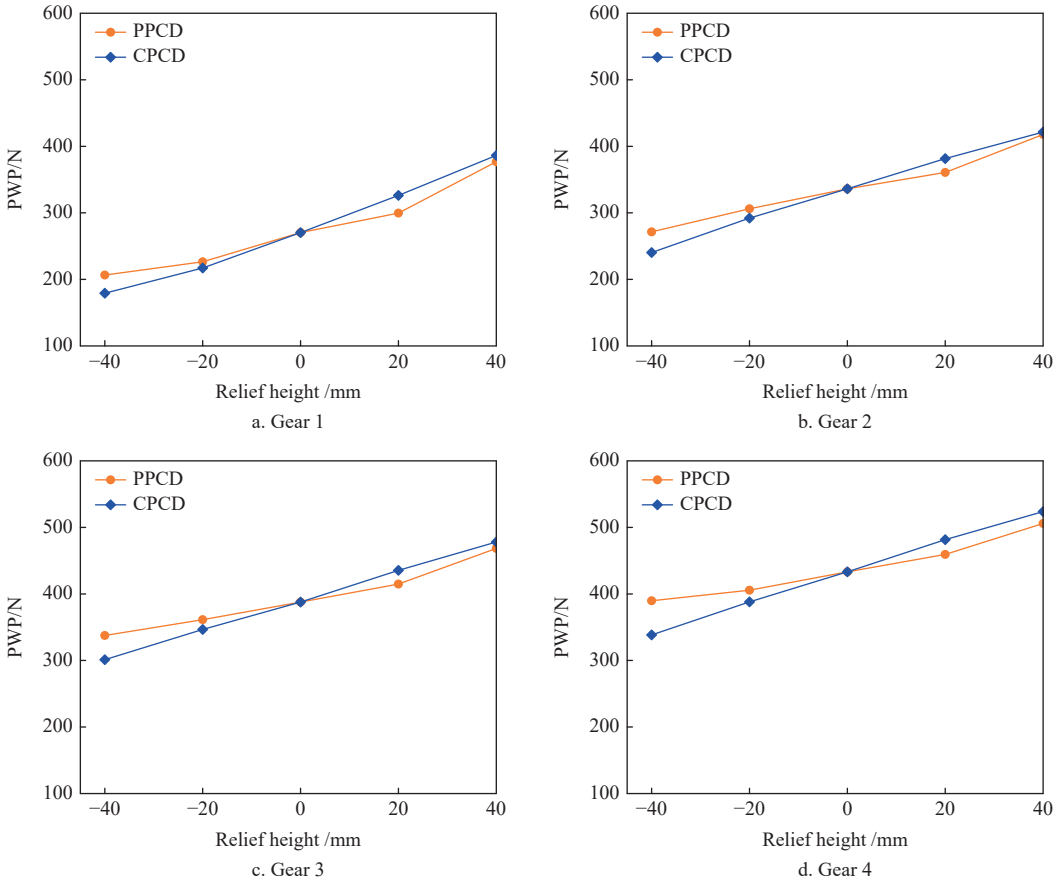


Figure 14 Comparison of PWP fluctuation

**Table 4 Comparison of the stiffness of the pressure device**

| Gear | Average stiffness/N·mm$^{-1}$ | |
|---|---|---|
| | Air spring | Coil spring |
| 1 | 2.13 | 2.59 |
| 2 | 1.83 | 2.27 |
| 3 | 1.64 | 2.21 |
| 4 | 1.45 | 2.32 |

undulating process of the press wheel as the test index, the quadratic rotation orthogonal combination finite element simulation test was carried out for each factor, and the optimal structural parameter combination of the air spring was determined: the piston radius was 27.2 mm, and the piston angle was 11.7°, the cord angle was 30.0°.

The bench test results showed that: the vertical stiffness simulation error was 7.1%, and the internal air pressure simulation error was 3.0%. The control response test showed that the average response time of the air spring inflating and deflating was 0.80 s, the maximum overshoot was 4.33% during inflation, and no pressure overshoot during deflation. The average reduction of the pneumatic pressure control device (PPCD) to pressure fluctuation was about 25.1%.

## Acknowledgements

This work was supported by the National Natural Science Foundation of China (Grant No. 52175260), Gratitude should be expressed to all the members of the Conservation Tillage Research Centre.

## [References]

[1] He J, Li H W, Chen H T, Lu C Y, Wang Q J. Research progress of conservation tillage technology and machine. Transactions of the CSAM, 2018; 49(4): 1–19. (in Chinese)

[2] Piazza G, Pellegrino E, Moscatelli M C, Ercoli L. Long-term conservation tillage and nitrogen fertilization effects on soil aggregate distribution, nutrient stocks and enzymatic activities in bulk soil and occluded microaggregates. Soil and Tillage Research, 2020; 196: 104482.

[3] Somasundaram J, Sinha N K, Dalal R C, Lal R, Mohanty M, Naorem A K, et al. No-till farming and conservation agriculture in South Asia-Issues, challenges, prospects and benefits. Critical Reviews in Plant Sciences, 2020; 39(3): 236–279.

[4] Yuan P P, Li H W, Lu C Y, Wang Q J, He J, Huang S H, et al. Design and experiment of seed furrow cleaning device based on throwing and sliding for no-till maize seeding. Int J Agric & Biol Eng, 2022; 15(4): 95–102.

[5] Fu W Q. Study on key technology of quality control for maize no-tillage drilling machinery. PhD dissertation. China Agricultural University, 2019; 136p. (in Chinese)

[6] Hu H N, Li H W, Wang Q J, He J, Lu C Y, Wang Y B, et al. Anti-blocking performance of ultrahigh-pressure waterjet assisted furrow opener for no-till seeder. Int J Agric & Biol Eng, 2020; 13(2): 64–70.

[7] Guo H. Study on maize sowing quality evaluation and soil covering-compacting device. PhD dissertation. Changchun: Jilin University, 2019; 141p. (in Chinese)

[8] Hartmann P, Zink A, Fleige H, Horn R. Effect of compaction, tillage and climate change on soil water balance of Arable Luvisols in Northwest Germany. Soil and Tillage Research, 2012; 124: 211–218.

[9] Zhang S L, Zhao W Y, Dai F, Song X F, Qu J F, Zhang F W. Simulation analysis and test on suppression operation process of ridging and film covering machine with full-film double-furrow. Transactions of the CSAE, 2020; 36(1): 20–30. (in Chinese)

[10] Taser O F, Kara O. Silage maize (*Zea mays* L. ) seedlings emergence as influenced by soil compaction treatments and contact pressures. Plant Soil and Environment, 2005; 51(7): 289–295.

[11] Jia H L, Guo H, Guo M Z, Wang L C, Zhao J L, Fan X H. Finite element analysis of performance on elastic press wheel of row sowing plow machine for covering with soil and its experiment. Transactions of the CSAE, 2015; 31(21): 9–16. (in Chinese)

[12] Guo H, Chen Z, Jia H L, Zheng T Z, Wang G, Wang Q. Design and experiment of soil-covering and soil-compacting device with cone-shaped

structure of wheel. Transactions of the CSAE, 2017; 33(12): 56–65. (in Chinese)

[13] Wang W J. Bionic press device with profiling mechanism for soybean precision planter. Master dissertation. Changchun: Jilin University, 2016; 97p. (in Chinese)

[14] Zhao S H, Liu H J, Tan H W, Yang Y Q, Zhang X M. Design and experiment of bidirectional profiling press device for hilly area. Transactions of the CSAM, 2017; 48(4): 82–89. (in Chinese)

[15] Hou S Y, Wei Z P, Shi N Y, Ji W Y, Zou Z. Design and parameter optimizing test of elastic spiral soil covering roller. Journal of Agricultural Mechanization Research, 2021; 43(3): 42–51. (in Chinese)

[16] Chen H T, Xu Y, Shi N Y. Design and experiment on three-way adjustable V-type soil-covering and soil-compacting device. Journal of Northeast Agricultural University, 2018; 49(11): 65–73. (in Chinese)

[17] Li B S, Tan Y, Chen J, Liu X X, Yang S H. Precise active seeding downforce control system based on fuzzy PID. Mathematical Problems in Engineering, 2020; 2020: 1–10.

[18] Bai H J, Fang X F, Wang D C, Yuan Y W, Zhou L M, Niu K. Design and test of control system for seeding depth and compaction of corn precision planter. Transactions of the CSAM, 2020; 51(9): 61–72. (in Chinese)

[19] Li B, Chen W W. Analysis and calculation of diaphragm air spring of an automobile. Journal of Hefei University of Technology, 2004; 10: 1191–1195. (in Chinese)

[20] Dugato D, Palma M-A-Z. Pressure and angle of the seed-fertilizer drill press wheel on corn emergence. Revista Brasileira de Engenharia Agrícola e Ambiental, 2018; 22(10): 726–731.

[21] Lu J. Design and optimization of heavy truck air suspension system. Qingdao University, 2019. (in Chinese)

[22] Yang Z B. Research on modeling and testing of bearing characteristics of vehicular rolling lobe air spring. Master dissertation. Guangzhou: South China University of Technology, 2018; 69p. (in Chinese)

[23] Chen D. The analysis of air-spring's stiffness on vehicle. Master dissertation. Chengdu: Southwest Jiaotong University, 2011; 86p. (in Chinese)

[24] Xu Y M, Hao W. Analysis on static mechanical properties of air spring based on ABAQUS. China Rubber Industry, 2015; 62(1): 41–44.

[25] Bester T, Oman S, Nagode M. Determining influential factors for an air spring fatigue life. Fatigue & Fracture of Engineering Materials & Structures, 2019; 42(1): 284–294.

[26] Wang H Y, He F, Zhao J, Cao H. Study on mechanical properties of air spring with auxiliary chamber based on fluid-solid coupling. China Rubber Industry, 2012; 59: 300–303. (in Chinese)

[27] Cao X P, Wang Q J, Xu D J, Huang S H, Wang X H, Wang L B. Design and analysis of pneumatic downforce regulating device for no-till corn planter. Agriculture, 2022; 12(10): 1513.